Multi-scale modelling of combined deterministic and stochastic fabric non-uniformity for realistic resin injection simulation

Endruweit, A.*, Zeng, X., Long, A.C.
Faculty of Engineering – Division of Materials, Mechanics & Structures, University of Nottingham, University Park, Nottingham, NG7 2RD, U.K.

*corresponding author,
e-mail andreas.endruweit@nottingham.ac.uk
tel. +44 (0)115 9514037

Abstract

The local fibre arrangement in a bi-directional fabric formed to a complex shape was modelled considering the stochastic arrangement of filaments within yarns, which determines axial and transverse yarn permeabilities, and the stochastic arrangement of yarns in a fabric, which determines the dimensions of inter-yarn gap spaces locally. To mimic the uncertainty in fabric forming, drape simulation was randomised in terms of start point and yarn start orientations. From yarn permeabilities and simulated local yarn spacing distributions, local fibre volume fractions and fabric permeabilities were approximated. This allowed resin injection into a deformed fabric to be simulated for different drape scenarios with different probabilities and different degrees of fabric randomness. The results indicate that variability in fabric properties and the forming process affects flow front shapes and times for complete impregnation of the reinforcement.

Keywords: Fabrics/textiles, Resin transfer moulding (RTM), permeability, drape, stochastic analysis

1 Introduction

In manufacture of polymer composite components employing Liquid Composite Moulding (LCM) processes, a fibrous reinforcement, preformed to the shape of the component, is impregnated with a liquid resin system. The impregnation is frequently modelled as flow of a viscous liquid through a porous medium, characterised by its porosity and permeability. Prediction of resin flow scenarios is straightforward if reinforcement porosity and permeability are uniform. However, in real reinforcements these properties typically show some degree of non-uniformity. For the most common type of reinforcement, bi-directional fabrics, two types of non-uniformity can be distinguished:

- Deterministic non-uniformity is related to the effect of drape, i.e. (localised) shear when the reinforcement is formed to a doubly-curved surface.
- Stochastic non-uniformity is related to material-inherent variability in the fabric structure, which is present even in undeformed flat fabric layers.

Due to both types of reinforcement non-uniformity, resin flow patterns and impregnation times in LCM-processing of actual components are hard to predict. Eventually, uncontrollable flow may result in incomplete impregnation and defect formation.

Regarding deterministic fabric non-uniformity, the mechanics of fabric drape [1,2], simulation of drape [3], and the effect of drape on the (local) fabric permeability [4-7] are discussed extensively in the literature. To address the issue of variability in resin flow patterns caused by stochastic local variations in fibre orientation and fibre volume fraction, Lundström et al. [8] derived non-uniform local fabric permeability values from variable dimensions of inter-yarn flow channels. This intrinsic non-uniformity of fabrics is related to the yarn mobility, which is determined by the fabric architecture [9]. The effect of random nesting may also contribute significantly if multiple fabric layers are used as reinforcement [10].

In a stochastic fabric model implemented by the authors [11], continuously varying yarn spacing was described by continuous functions with random parameters, which were related to experimentally quantified fibre angle variations in undeformed fabrics. These allowed local fabric properties to be derived as input for resin injection simulations. From the simulation results, probable outcomes of resin injections were deduced for flat textiles with non-uniform properties. Predicted flow front shapes were in qualitative agreement with experimental observations, and global permeabilities and permeabiliy variations, predicted based on series of simulations, were found to be in the order of magnitude of typical experimental results.

In this study, resin injection into preforms with arbitrary complex geometry is simulated based on local fabric permeability fields, which are modelled by combining drape simulation with the following stochastic effects:

- at the micro-scale: random arrangement of filaments in yarns;
- at the meso-scale: random variations in local yarn spacing in unsheared fabric;
- at the macro-/meso-scale: variability in forming start point and yarn start orientations, determining yarn paths and shear angles.

The aim is to predict typical resin injection scenarios for reinforcements with realistic non-uniformity in order to optimise process parameters for production of composite components applying LCM-technology, in particular location of injection gates and vents in the mould to achieve complete impregnation, i.e. high quality, of finished components.

2 Fabric modelling

2.1 General approach

To model the local meso-scale structure in a non-uniform draped fabric, fabric drape simulation and randomisation of the yarn spacing are combined. Fabric shear and random

yarn waviness both affect the local yarn spacing and hence are competing effects. In unsheared flat bi-directional fabrics, measured angles between warp- and weft-yarns were found to be normally distributed [12] reflecting some degree of in-plane yarn waviness. This is related to continuous variations in local yarn spacing along each fabric direction. When the fabric is sheared, the (average) yarn spacing is reduced, which results in a reduction in yarn mobility. Where adjacent wavy yarns are in contact with each other locally, lateral forces straighten the yarns, thus reducing variability in the fabric structure. This implies that warp- and weft-yarns slide over each other (with friction) in the cross-over points, i.e. the distance between cross-over points changes. Forming of a fabric showing this type of behaviour was simulated by Skordos and Sutcliffe, who modelled a bi-directional fabric with stochastic geometrical parameters and then calculated local deformation employing a non-linear finite element method [13]. This approach reproduces the behaviour of the fabric accurately, but implies a complex and computationally expensive solution procedure.

Here, a kinematic pin-jointed net approach is employed to reduce the computational cost for forming simulation. Since a pin-jointed net model requires uniform edge length in the draped net [14], in a first step, drape is simulated for an idealised uniform fabric. Fabric randomisation is then applied based on the local residual inter-yarn gap width derived from the drape simulation. This allows the mechanics of yarn slippage in cross-over points to be ignored to reduce the complexity of the forming problem. Since drape and randomisation both affect yarn spacing in the same way, inversion of the sequence appears admissible.

In addition to fabric non-uniformity, the uncertainty in initial conditions for the fabric forming process is considered here. Thus, the proposed approach for LCM process simulation implies the following steps:

1. Discretisation of the geometry of the finished component into finite elements
2. Randomisation of the initial conditions for drape simulation

3. Drape simulation employing a “pin-jointed net” method
4. Randomisation of local fabric properties (according to outcome of drape simulation)
5. Calculation of the local permeability field
6. Resin injection simulation employing a finite element (Darcy) solver

2.2 Randomised drape simulation

Forming of bi-directional fabrics was simulated using the kinematic code DrapeIt, which was developed at Nottingham University. Based on a geometrical model of the finished component, represented by a doubly-curved surface consisting of triangular flat patches (which coincide with the finite elements for flow simulation), a pin-jointed net approach is implemented. This implies that start point and start directions for yarns in both fabric directions are set, and two seed yarn paths are generated by projection onto the surface (along the global co-ordinate *z*-axis), separating the geometry into four quadrants [15]. Connected yarn segments with fixed length, corresponding to the spacing between yarn cross-over points, are placed sequentially on the geometry to populate each quadrant.

Outputs of the drape simulation are

- two vectors, $\mathbf{e}_{warp}$ and $\mathbf{e}_{weft}$, for each surface patch (finite element), indicating local fabric warp- and weft-directions,
- co-ordinates of yarn cross-over points (Fig. 1), which are indexed by positive integers, *i* and *j*, in each quadrant of the drape geometry relative to the start point at (0, 0).

To mimic the uncertainty in placing a dry reinforcement in a tool as start for the following deterministic forming process, which was studied by Elkington et al. [16] for manual prepreg lay-up but occurs similarly in automated prefoming processes, the drape simulation was randomised in terms of start point and yarn start orientations. For a given target start point and target start orientations, the angle between the fabric warp- and weft- direction at the start

point is assumed to be 90°, and the yarn start orientations are assumed to be normally distributed around the target orientation (0°). In addition, the distance between the target start point and the actual start point, projected onto a plane normal to the direction of fabric deposition onto the actual surface, is assumed to be normally distributed. The probability for the actual start point to be found is equal in any direction relative to the target start point.

If the fabric is formed by applying a force along the global co-ordinate *z*-axis, this assumption can be formulated in terms of the probability for the start point to be found in the surface element dA_{xy} at a position (x,y) in the x-y-plane,

$$dP_{xy} = \frac{1}{2\pi\sigma_x^2}\exp\left(-\frac{1}{2}\left(\left(\frac{x}{\sigma_x}\right)^2+\left(\frac{y}{\sigma_x}\right)^2\right)\right)dA_{xy} \quad , \tag{1}$$

where σ_x is the standard deviation of the normal distribution. Since the orientation of a surface element, dA, anywhere on the geometry can be described by the angle β included by the surface normal vectors in dA and in the target start point, dA_{xy} and dA are correlated via

$$dA_{xy} = dA\cos\beta \quad . \tag{2}$$

Thus, the probability, dP, for the start point to be found in the surface element dA anywhere on the geometry can be obtained by substituting Eq. (2) into Eq. (1) and introducing a corrective factor to take into account the total surface area of the geometry. Effectively, the probability decreases not only with increasing distance from the target start point, but also with increasing angle between the local surface normal and the surface normal in the target start point.

For the following calculations of the local permeability, it is assumed that the angle between both yarn directions in the original unsheared fabric, α_0, is 90°. The yarn spacing, A_0, and yarn dimensions, described by the original in-plane yarn halfwidth of the unsheared fabric, R_p, are assumed to be identical in both fabric directions. For each triangular finite element for flow simulation, the local fibre angle is determined from the direction vectors

generated in the drape simulation. From the yarn spacing in the unsheared fabric, A_0, and the local fibre angle, α, which is defined such that $\alpha \leq 90°$, the distance, a_0, between yarn axes which are assumed to be locally parallel (Fig. 2), is determined as

$$a_0 = A_0 \cos(90° - \alpha) \quad . \tag{3}$$

If $a_0 > 2R_p$, i.e. adjacent yarns are not in contact after shearing the fabric, the local yarn mobility can be assumed to be high, and the yarn spacing is randomised as described in Section 2.3. If $a_0 \leq 2R_p$, i.e. adjacent yarns are already in contact locally, and (further) lateral yarn compression would be required to change the yarn spacing, the randomisation procedure is skipped, and the permeability is calculated as described in Section 3 for values of a and b both set to a_0.

2.3 Fabric randomisation

Here, a bi-directional fabric is treated as a structure with two independent uni-directional layers, similar to a non-crimp fabric (NCF). The variable yarn spacing in the layers representing the warp- and weft-direction, a and b, is determined from a_0 and random parameters. Methods for description of yarn waviness in bi-directional fabrics were proposed by Ghanem and Dham [17] and Yushanov and Bogdanovich [18]. Adapting the former method, Endruweit and Long [11] modelled continuously varying spacing of locally parallel yarns in a planar fabric, where the fabric directions are aligned with the x- and y-directions. Hence, a, varying along the x-direction, and b, varying along the y-direction, were described by

$$a - 2R_p = (a_0 - 2R_p)\left(1 + \frac{1}{N}\sum_{i=0}^{N-1} w_i(x)\, w_i(y)\right) \tag{4}$$

and

$$b - 2R_p = (a_0 - 2R_p)\left(1 + \frac{1}{N}\sum_{i=0}^{N-1} w_i(x)\, w_i(y)\right) \quad . \tag{5}$$

In the functions

$$w_i(x) = \sin(\omega_{ai}\, x + \varphi_{ai}) \tag{6}$$

and

$$w_i(y) = \sin(\omega_{bi}\, y + \varphi_{bi}) \quad , \tag{7}$$

the values of the frequencies ω_{ai} and ω_{bi} and the phases φ_{ai} and φ_{bi}, which describe the in-plane fibre tow waviness, are determined stochastically. A revised version of the proposed method [11] is employed here. While the phases are assumed to be uniformly distributed on the interval between 0 and π, each frequency is correlated to an angle, $\Delta\alpha$, describing the deviation in yarn alignment from the nominal direction according to

$$\omega = \left| \frac{\tan\Delta\alpha}{A_0 - 2R_p} \right| \quad . \tag{8}$$

Since measured fibre angles in actual unsheared fabrics were found to be normally distributed with standard deviation σ_α [12], the probability density of $\Delta\alpha$ is

$$P(\Delta\alpha) = \frac{1}{\sigma_\alpha \sqrt{2\pi}} \exp\left(-\frac{\Delta\alpha^2}{2\sigma_\alpha^2}\right) \quad . \tag{9}$$

The probability to find a deviation in yarn alignment characterised by an angle smaller than or equal to $\Delta\alpha$ is described by the cumulative distribution function

$$D(\Delta\alpha) = \frac{1}{2}\left(1 + \mathrm{erf}\left(\frac{\Delta\alpha}{\sigma_\alpha \sqrt{2}}\right)\right) \quad , \tag{10}$$

where

$$\mathrm{erf}(z) = \frac{2}{\sqrt{\pi}} \int_0^z \exp(-t^2)\, dt \tag{11}$$

is the error function. By inverting Eq. (10), normally distributed values for $\Delta\alpha$ can be generated from uniformly distributed random values, D, on the interval (0,1) via

$$\Delta\alpha = \sigma_\alpha \sqrt{2}\,\mathrm{erf}^{-1}(2D-1) \quad , \tag{12}$$

where the inverse error function, erf^{-1}, can be approximated by a power series [19]. Based on these values of $\Delta\alpha$, frequencies for modelling yarn waviness are sampled according to Eq. (8). This implies that the probability for a frequency to occur decreases with increasing value of ω, thus deviating from the original approach proposed by the authors [11].

In Eqs. (4) and (5), N was set to a value of 6 as a compromise between accurate reproduction of the distribution of frequencies and computational efficiency. The choice of terms in the expansions implies that the waviness along the yarn directions determines the scale of variation perpendicular to the yarns as well. Since the changes in yarn spacing are limited by the yarn mobility in the transverse direction, the amplitudes of the waviness are normalised by the number of terms in the expansion, N. This limitation on the waviness implies that the global superficial density of the fabric remains constant.

Continuous co-ordinates, x and y, were used for description of a and b in a planar system [11]. To assign properties to finite elements for flow simulation, a and b were picked at the centre of mass (x_{cm}, y_{cm}) of each finite element. To extend the approach to the more complex case of doubly-curved surfaces, the continuous co-ordinates are replaced by discrete co-ordinates $n_{warp}A_0$ and $n_{weft}A_0$. Here, the unique signed integers n_{warp} and n_{weft} (Table 1) are derived from the positive integers i and j, which index the positions of yarn cross-over points along the fabric warp- and weft-direction in each quadrant of the geometry (and thus are not unique) relative to the start point of drape at (0, 0). For each finite element, a and b are calculated according to Eq. (4) and (5) with a_0 determined according to Eq. (3). The functions $w_i(n_{warp}A_0)$ and $w_i(n_{weft}A_0)$ are evaluated at the yarn cross-over point (n_{warp}, n_{weft}) nearest to the centre of mass, which is determined from the co-ordinates of the three nodes of the element.

This approach effectively maps the continuously varying yarn spacing in the undeformed fabric onto a doubly-curved surface.

3 Local permeability calculation

3.1 General approach

To estimate the permeability for each finite element, the local fabric structure is assumed to be of the type illustrated in Fig. 3 (similar to a NCF). The yarns in both fabric directions are assumed to be piecewise parallel with spacing a and b, the local values of which are generated as described above. For each of the two layers of yarns in the fabric, the permeability is estimated separately. The layer permeability parallel to the yarn axis is calculated from the yarn permeability and the equivalent permeability of the inter-yarn gap, applying a rule of mixture according to the percentage of layer cross-section occupied by the gap, Φ. The transverse layer permeability is dominated by the transverse yarn permeability. The fabric permeability is calculated from thickness-weighted averaging of the layer permeabilities.

In the following, permeability calculation will be illustrated for the layer containing yarns oriented along the fabric warp-direction, where the geometry is characterised by the yarn spacing, a, the yarn thickness, h, and the halfwidth, R_p, of the uncompressed yarn. Local random variations in yarn cross-sectional shapes in real fabrics were studied by Olave et al. [20]. While irregular non-symmetrical shapes can currently not be handled and are not considered here, variations in simplified yarn cross-sections due to local lateral compression are approximated. Estimation of yarn cross-sections, which typically show characteristics of elliptical, lenticular and rectangular shapes, and numerical calculation of the equivalent permeability of inter-yarn gaps as demonstrated by Nordlund and Lundström [21] is too complex and time-consuming to be employed for each finite element individually. Hence,

three general cases for layers of yarns, distinguished by the ratio $2R_p/a$ and the value of Φ (Fig. 3), are analysed here.

Case 1: $2R_p < a$ and $\Phi > 0$

- The layer has a dual-scale structure (gaps between yarns),
- yarns have the initial cross-sectional shape as in the undeformed fabric, which is assumed to be elliptical with halfwidth $R_e = R_p$,
- the fibre volume fraction in the yarns has the initial value, V_{f0}.

Case 2: $2R_p \geq a$ and $\Phi > 0$

- The layer has a dual-scale structure (gaps between yarns),
- yarn cross-sections are assumed to be power-ellipses [22] with halfwidth smaller than R_p,
- the fibre volume fraction in the yarns has the initial value, V_{f0}.

Case 3: $2R_p \geq a$ and $\Phi = 0$

- The layer has a single-scale structure (gaps are closed),
- yarn cross-sections are assumed to be rectangular with halfwidth smaller than R_p,
- the fibre volume fraction in the yarns has a value $V_{fyarn} \geq V_{f0}$.

Walther et al. [23] modelled a draped fabric with dual-scale porosity, as in cases 1 and 2, as a homogeneous single-scale medium with additional sink terms representing the porous yarns. Here, the dual-scale structure and the transition to single-scale at $\Phi = 0$ is reproduced explicitly in the permeability model.

3.2 Equivalent permeability of inter-yarn gaps

The axial equivalent permeability of a layer with inter-yarn gap can be approximated as

$$K = \frac{2 D_h^2 \Phi}{c} \quad , \tag{13}$$

where D_h is the hydraulic diameter of the gap, Φ the percentage of total cross-sectional layer area occupied by the gap, and c a friction factor related to the shape of the gap [24]. The contribution of axial yarn permeabilities to the layer permeability is generally small compared to the contribution of the equivalent gap permeability and is neglected at this stage. The hydraulic diameter is defined as

$$D_h = \frac{4Q}{U} \quad , \tag{14}$$

where Q is the gap cross-sectional area and U the gap perimeter in cross-section.

For case 1 and elliptical yarns, the cross-sectional area of inter-yarn gaps is

$$Q_e = (a - \tfrac{1}{2}\pi R_e)\, h \quad . \tag{15}$$

Using Ramanujan's approximation for the perimeter of an ellipse [25], the gap perimeter can be estimated as

$$U_e = 2a + \pi\left(3(R_e + \tfrac{1}{2}h) - \sqrt{5R_e\, h + 3(R_e^2 + \tfrac{1}{4}h^2)}\right) \quad . \tag{16}$$

The percentage Φ is

$$\Phi_e = 1 - \frac{\pi R_e}{2a} \quad . \tag{17}$$

Determination of the friction factor, c, is non-trivial. For characterisation of flow through a duct with arbitrary cross-section, Mortensen et al. [26] introduced a geometrical correction factor, here referred to as

$$\gamma = \frac{\Delta p\, Q}{v\, \eta\, L} \quad , \tag{18}$$

and the dimensionless compactness of the duct,

$$C = \frac{U^2}{Q} \quad , \tag{19}$$

where L is the length of the duct, Δp the pressure drop along L, v the average flow velocity, and η the fluid viscosity. Comparing Eq. (18) with Darcy's law, which (for the 1D case) can be expressed as

$$v = \frac{K \Delta p}{\eta L} \quad , \tag{20}$$

implies that

$$K = \frac{Q}{\gamma} \quad . \tag{21}$$

Equating this with the equivalent duct permeability [24],

$$K = \frac{2 D_h^2}{c} \quad , \tag{22}$$

allows c to be expressed as

$$c = \frac{32 \gamma}{C} \quad . \tag{23}$$

For elliptical yarns, C can be related to the geometrical parameters of the flow channel by substitution of U and Q, which are calculated according to Eqs. (15) and (16). To determine γ for different values of C, Computational Fluid Dynamics (CFD) simulations of steady state laminar flow were run in Ansys® CFX®. For an applied pressure drop, the average axial flow velocity in flow channels as shown in Fig. 3 (top right) was computed. Translational periodicity was applied along the yarn direction to represent parallel yarns with constant cross-section. The flow channel perimeter was assumed to be impermeable, and non-slip wall boundary conditions were applied. A mesh sensitivity study indicated that the solution converged if the average edge length of finite elements in the CFD simulations was 0.01 mm or less. The average flow velocity obtained from the simulations allowed the equivalent axial channel permeability to be determined according to Eq. (20). Then, γ was calculated according to Eq. (21). Results for three different percentages, Φ_e, as defined in Eq. (17), are

plotted in Fig. 4. Here, aspect ratios of elliptical yarns were considered in the range $2R_e/h > 1$. As described by Mortensen et al. [26] for different duct geometries, the dependence of γ on C is linear at each percentage, Φ_e. Different equations for $\gamma(C)$ are related to different flow velocity distributions across the gap cross-section for different Φ_e, as illustrated for two examples in Fig. 5.

Substituting relations for γ into Eq. (23) allows the friction factor, c, to be described as a function of C only. Its dependence on the aspect ratio, $2R_e/h$, of elliptical yarns (Fig. 6) can be approximated as

$$c_e = B_1 (2 R_e / h)^{-B_2} \quad , \tag{24}$$

where

$$B_1 = 7.83 \Phi_e^{-2.22} \tag{25}$$

and

$$B_2 = 0.031 \Phi_e^{-2.51} \quad . \tag{26}$$

Equation (24) allows the axial permeability of a gap between two yarns with elliptical cross-section to be approximated analytically, which can be used to estimate the axial layer permeability according to Eq. (13). Since it proves difficult to determine the transverse permeability of a layer of elliptical yarns, the cross-sections are converted to equivalent rectangular shapes (Fig. 7). This geometrical simplification facilitates transverse permeability estimation for yarns and inter-yarn gaps.

If the yarns are assumed to be rectangular, the gap cross-sectional area is

$$Q_r = (a - 2 R_r) h \quad , \tag{27}$$

and the gap perimeter is

$$U_r = 2 h + 2 (a - 2 R_r) \quad , \tag{28}$$

where R_r is the halfwidth of the yarns. The percentage of total cross-sectional layer area occupied by the gap is

$$\Phi_r = 1 - \frac{2R_r}{a} \quad . \tag{29}$$

The approximation for the friction factor

$$c_r = 56.4 R^{0.17} \quad , \tag{30}$$

where

$$R = \begin{cases} h/(2(a-2R_r)) \text{ , if } 2(a-2R_r) \le h \\ 2(a-2R_r)/h \text{ , if } 2(a-2R_r) > h \end{cases} \quad , \tag{31}$$

was derived based on data for ducts with rectangular cross-section tabulated by White [27] and plotted in Fig. 8.

Equating axial permeabilities for layers of elliptical yarns and rectangular yarns, calculated according to Eq. (13) with the derived approximations for c_e and c_r, allows R_r to be estimated as a function of a, h and R_e. Conversion of the yarn shape from elliptical to rectangular is based on equating axial layer permeabilities because they are highly sensitive to the influence of the inter-yarn gap shape, while transverse layer permeabilities are determined mainly by yarn permeabilities.

For case 3, all inter-yarn gaps are closed, and the compressed yarns have rectangular cross-section. Here, $R_r = a/2$ corresponds to the actual yarn halfwidth.

For case 2 with $2R_p \ge a$, yarns are deformed in lateral compression. Resulting yarn cross-sectional shapes can be approximated as power ellipses as discussed elsewhere [22]. Since determining Q and U for power ellipses is difficult, the approach described above (for $2R_p \le a$) cannot be applied. Here, the dependence of R_r on R_e is approximated by linear interpolation between the value of R_r at $2R_e = a$ (calculated as described above) and $R_r = a/2$ at $2R_e/a = 4/\pi$, which corresponds to the condition that all inter-yarn gaps disappear at $a =$

$R_e\pi/2$. Since the dependence of R_r on R_e (Fig. 9) is weak in this range, the error induced by this approximation is small.

It is to be noted that the total fibre volume in each cell is not necessarily conserved in the conversion from elliptical to rectangular yarns, as long as there is an inter-yarn gap. This is considered acceptable, since the permeability is gap-dominated. On the other hand, the total fibre volume is conserved, if all gaps are closed. This is important, since the permeability is yarn-dominated in this range. In the following, the in-plane yarn dimension will be expressed in terms of the transformed rectangular halfwidth, R_r.

3.3 Yarn permeability

The principal permeability values of a yarn, k_{yarn1} (parallel to its axis) and k_{yarn2} (perpendicular to its axis), at a fibre volume fraction V_{fyarn} are estimated based on the equations derived by Gebart [24] from Eq. (13),

$$k_{yarn1} = \frac{R_f^2}{4c_1} \frac{(1-V_{fyarn})^3}{V_{fyarn}^2} \tag{32}$$

and

$$k_{yarn2} = c_2 \left(\sqrt{\frac{V_{f\max}}{V_{fyarn}}} - 1 \right)^{5/2} R_f^2 \ , \tag{33}$$

where c_1, c_2, V_{fmax} and R_f are geometrical parameters. Values for c_1 and c_2 were estimated by Gebart based on the assumption of perfectly uniform filament arrangements. However, the arrangement of filaments within yarns is typically non-uniform [28], and, at given fibre volume fraction, permeabilities for non-uniform yarns differ significantly from idealised permeabilities for uniform yarns. Here, the parameters in Gebart's equations were estimated (Table 2) based on numerically generated results for permeabilities of yarns with non-uniform filament arrangement [22]. A potential change in the yarn-scale values of c_1 and c_2

due to filament reordering with increasing V_{fyarn} was neglected here, although a reduction in non-uniformity can be expected.

For the example of a uni-directional carbon fibre reinforcement with a filament count of 12K, the typical fibre volume fraction in the yarns, V_{fyarn}, was found to be constant at approximately 0.65 at low compression levels [22]. At high levels of compression, V_{fyarn} was found to increase. This reflects compression mechanisms for woven fabrics discussed by Potluri and Sagar [29]. They are, in sequence of their onset, change of crimp by fibre bending (does not apply to the model here), closing of gaps in the fabric structure (at approximately constant V_{fyarn}), and change of yarn cross-sections by micro-scale filament reordering (i.e. increase in V_{fyarn}). Here, V_{fyarn} is assumed to be constant at a value $V_{f0} = 0.65$ for cases 1 and 2.

For case 3, where $a = 2R_r$, there is no inter-yarn gap, i.e. the layer makes the transition from dual-scale to single-scale porous medium. Due to lateral yarn compression and reduction in yarn halfwidth with decreasing a, V_{fyarn} is changes according to

$$V_{fyarn} = \frac{V_{f0}\,\pi\,R_e}{2\,a} \quad . \tag{34}$$

The maximum value of V_{fyarn} is enforced to the theoretically possible maximum of 0.91 if the calculated value is greater than this. A potential increase in yarn thickness is not considered here.

3.4 Layer permeability

The effective longitudinal layer permeability is calculated from the individual permeabilities of yarns (with rectangular cross-section) and inter-yarn gaps in parallel, ignoring the potential exchange of fluid between the open inter-yarn gap and the porous yarns:

$$k_{layer1} = \frac{a - 2R_r}{a} k_{gap1} + \frac{2R_r}{a} k_{yarn1} \quad . \tag{35}$$

The effective transverse layer permeability is calculated from the individual permeabilites in series:

$$k_{layer2} = \frac{a\, k_{gap2}\, k_{yarn2}}{2R_r\, k_{gap2} + (a - 2R_r)\, k_{yarn2}} \quad . \tag{36}$$

This can be approximated as

$$k_{layer2} \approx \frac{a\, k_{yarn2}}{2R_r} \quad . \tag{37}$$

In Eq. (35), the equivalent permeability of the inter-yarn gap can be estimated according to Eq. (22) with values for *c* given by White [27]. Alternatively, it can be approximated as

$$k_{gap1} = \frac{h^2}{12}\left(1 - \frac{192\,h}{\pi^5 (a - 2R_r)} \sum_{i=1,3,5\ldots}^{\infty} \frac{\tanh(i\pi (a - 2R_r)/2h)}{i^5}\right) \quad , \tag{38}$$

which is the solution of the Navier-Stokes equation for flow through a rectangular duct with no-slip boundary conditions for solid (top, representing tool surface, and bottom, representing interface to weft-layer, in Fig. 7) and permeable (left and right, representing interfaces to porous yarns) walls [30]. When the sum in Eq. (38) is truncated after the first three terms, which was found to cause a negligible error, results for several examples differed by no more than 0.5 % from results calculated according to Eq. (22).

For case 3, Eqs. (35) and (37) simplify, since $2R_r = a$, and the layer permeabilites are equal to the respective yarn permabilities. These are calculated from Eqs. (32) and (33) using the new value for V_{fyarn} according to Eq. (34) rather than V_{f0}.

Examples for layer permeabilities, k_{layer1} and k_{layer2}, are plotted in Fig. 10 as functions of the ratio, $2R_e/a$. The same applies to the yarn layer in the fabric weft-direction with yarn spacing, *b*. The results in Fig. 10 show a strong increase in longitudinal layer permeability if

the inter-yarn gap width is increased, but only a relatively weak dependence of the transverse permeability on the gap width.

3.5 Fabric permeability

Ignoring inter-layer fluid exchange, the permeability tensor of the combined layers is calculated by thickness-weighted averaging of the basic permeabilites of the individual layers in both fabric directions according to

$$\mathbf{K}(\theta) = \frac{\mathbf{k}_{warp}(\theta) + \mathbf{k}_{weft}(\alpha - \theta)}{2} \quad , \tag{39}$$

where θ is the angle between the fabric warp-direction and the direction of the principal permeability value, K_1. The angle θ is determined from the condition that off-diagonal elements in the tensor for the principal permeability are zero:

$$0 = (k_{warp2} - k_{warp1}) \sin\theta \cos\theta + (k_{weft2} - k_{weft1}) \sin(\alpha - \theta) \cos(\alpha - \theta) \quad . \tag{40}$$

In Fig. 11, θ is plotted as a function of the fibre angle, α, for different ratios k_{warp1}/k_{weft1}. The results are very similar to an empirical relation derived by Endruweit and Ermanni [31] for sheared fabrics at different levels of anisotropy.

With the value for θ, the principal permeability values are calculated according to

$$K_1 = (k_{warp1} \cos^2\theta + k_{warp2} \sin^2\theta + k_{weft1} \cos^2(\alpha - \theta) + k_{weft2} \sin^2(\alpha - \theta)) / 2 \tag{41}$$

and

$$K_2 = (k_{warp2} \cos^2\theta + k_{warp1} \sin^2\theta + k_{weft2} \cos^2(\alpha - \theta) + k_{weft1} \sin^2(\alpha - \theta)) / 2 \quad . \tag{42}$$

The unit vector, $\mathbf{e}_1$, for the directions of the principal permeability, K_1, is calculated from

$$\mathbf{e}_1 = E_{warp}\, \mathbf{e}_{warp} + E_{weft}\, \mathbf{e}_{weft} \quad , \tag{43}$$

where

$$\mathbf{e}_{warp}\, \mathbf{e}_1 = \cos\theta \tag{44}$$

and

$$\mathbf{e}_{weft}\,\mathbf{e}_1 = \cos(\alpha - \theta) \quad . \tag{45}$$

Solving this system of three equations allows the factors, E_{warp} and E_{weft}, in Eq. (43) to be determined as

$$E_{warp} = \cos\theta - E_{weft}\cos\alpha \tag{46}$$

and

$$E_{weft} = \frac{\cos(\alpha - \theta) - \cos\theta\cos\alpha}{\sin^2\alpha} \quad . \tag{47}$$

Similarly, the system of equations

$$\mathbf{e}_2 = G_{warp}\,\mathbf{e}_{warp} + G_{weft}\,\mathbf{e}_{weft} \quad , \tag{48}$$

$$\mathbf{e}_{warp}\,\mathbf{e}_2 = \cos(\theta + 90°) \tag{49}$$

and

$$\mathbf{e}_{weft}\,\mathbf{e}_2 = \cos(90° - \alpha + \theta) \quad , \tag{50}$$

allows the factors, G_{warp} and G_{weft}, for calculation of $\mathbf{e}_2$ according to Eq. (48) to be determined as

$$G_{warp} = \cos(\theta + 90°) - G_{weft}\cos\alpha \tag{51}$$

and

$$G_{weft} = \frac{\cos(90° - \alpha + \theta) - \cos(\theta + 90°)\cos\alpha}{\sin^2\alpha} \quad . \tag{52}$$

The fibre volume fraction in the fabric is

$$V_f = \frac{F_{warp}\,V_{fwarp}}{2} + \frac{F_{weft}\,V_{fweft}}{2} \tag{53}$$

where V_{fwarp} and V_{fweft} are the fibre volume fractions in yarns, V_{fyarn}, in the layers in warp- and weft-direction, respectively. The factors F_{warp} and F_{weft} indicate the yarn content in both layers. Their values are

$$F_{warp} = \begin{cases} 2R_r / a \text{ , if } a > 2R_r \\ 1, \text{if } a \le 2R_r \end{cases} \tag{54}$$

and

$$F_{weft} = \begin{cases} 2R_r / b \text{ , if } b > 2R_r \\ 1, \text{if } b \le 2R_r \end{cases} . \tag{55}$$

4 Application

For demonstration of the methodology proposed above, resin injection into a fabric formed to the double-dome forming benchmark geometry [32] was simulated. The equations describing unsaturated flow of a viscous liquid through a porous medium considering conservation of the fluid mass were solved based on a non-conforming finite element method [33], which is implemented in the commercial software PAM-RTM^{TM}. The double-dome geometry was discretised into 9420 triangular finite elements. One set of local fabric properties was attributed to each finite element. The typical edge length of the finite elements (approximately 3.9 mm) is slightly longer than the yarn spacing, A_0, for the example discussed here (Table 3). Hence, the local fabric structure (Fig. 3) can be homogenised for each finite element.

The local properties were calculated based on the assumption that the fabric architecture in the undeformed uniform fabric is characterised by the geometrical parameters listed in Table 3. From the condition $a_0 = 2R_p$, Eq. (3) allows the fibre angle at zero width of inter-yarn gaps to be determined as $\alpha_1 = 56°$. Based on Eq. (34), the minimum fibre angle that can be obtained (when V_{fyarn} has the maximum theoretically possible value of 0.91) can be calculated as $\alpha_2 = 37°$. Three levels of material-inherent non-uniformity of the undeformed fabric were considered. These examples were characterised by standard deviations of fibre angle

distributions, σ_α, with values 0.0° (uniform fabric), 2.5° and 5.0°. The values of these parameters lie in a realistic range.

Three example scenarios for randomised drape simulation are considered here, “on target”, “likely” and “unlikely”. These scenarios are characterised by the parameters listed in Table 4. For illustration, relative probabilities for the drape start point to be found at the respective positions were calculated according to Eq. (1) for the example with σ_x = 50 mm which is thought to be in a realistic order of magnitude. The deviation from the target orientation indicates the angle between the actual fibre directions in the start point and the co-ordinate *x*- and *y*-direction, i.e. the axes of the geometry. The respective shear angle distributions are plotted in Fig. 12. Since the example geometry is flat around the target start point, the configuration of the draped fabric is insensitive to small deviations in the forming process from the target. Hence, the “on target” and “likely” scenarios are almost identical. In both cases, fabric shear is restricted mainly to the hemispherical parts of the geometry. However, the shear angle distribution in the “unlikely” drape scenario is asymmetrical and shows zones of relatively high shear even in flat sections of the geometry.

For the nine possible combinations of the three values for σ_α (0.0°, 2.5° and 5.0°) and the three drape scenarios in Fig. 12, permeability fields were generated, and radial injection (from the centre of the geometry) of a fluid with a viscosity of 0.1 Pa×s at a constant injection pressure of 1 bar was simulated. For $\sigma_\alpha \neq 0.0°$, five instances were analysed for each combination of parameters. For each combination, flow front patterns may vary significantly, which is reflected in the standard deviations in the total fill times in Table 5. Representative flow front patterns, i.e. patterns corresponding to fill times close to the average for each case (Table 5), exhibit slight non-symmetry relative to the co-ordinate *x*-axis (Fig. 13), even for drape “on target” with no fabric variability. This can be explained by the limited numerical accuracy in the geometrical data (the shear angle distribution “on target” is also not perfectly

symmetrical). If only drape is considered for local permeability modelling (σ_α = 0.0°), there is almost no difference between the scenarios “on target” and “likely” since the shear angle distributions are very similar. The points in the fabric which take longest to impregnate coincide with zones of high shear angles. For the “unlikely” drape scenario, flow front ellipses are rotated counter-clockwise, and the flow front propagation is significantly slower in the *y*-direction compared to the other two cases. These observations are plausible considering the shear angle distributions in Fig. 12, where the “unlikely” drape scenario shows zones of relatively high shear, i.e. low permeability, roughly aligned with the *x*-direction.

According to Eq. (8), the probability to find high frequency yarn waviness is higher for σ_α = 5.0° than for σ_α = 2.5°. Hence, local permeabilities tend to vary on a smaller scale for σ_α = 5.0° than for σ_α = 2.5°. Qualitatively, this is reflected in the size of anomalies on the flow fronts, which appears to decrease with increasing σ_α.

Quantitatively, simulation results are compared in terms of fill times in Table 5. For “on target” and “likely” drape scenarios, the average fill time decreases when σ_α is increased from 0.0° to 2.5°. For σ_α = 5.0° it increases again to a level similar to the fill time for σ_α = 0.0°. This is consistent with simulation results for a non-uniform flat fabric generated using the original model for fabric randomisation [11]. Average fill times were observed to deviate from results for the uniform case for small σ_α, i.e. large wavelength of yarn waviness, but were almost identical to those for the uniform fabric for increasing σ_α, i.e. decreasing wavelength. The observation was explained by the dominating wavelength in the simulated yarn waviness, which, at minimum fill time, was in the same order of magnitude as the dimensions of the geometry, hence allowing local permeability maxima to stretch across the entire geometry. In Fig. 13, this is reflected in the elongation of the respective flow fronts along the *y*-direction. For the “unlikely” drape scenario, there appears to be no clear

dependence of the average fill time on σ_α. The average fill time tends to increase with increasing deviation in the drape configuration from the target situation. This suggests that for drape “on target”, results are dominated by the fabric randomisation, for the “unlikely” case, results are dominated by fabric drape. No clear trend can be identified for the variability in fill time, although (based on the qualitative observation described above) it might be expected to decrease with increasing σ_α.

The formation of dry spots during reinforcement impregnation is related to the presence of low permeability spots where the local (meso-scale) flow velocity is reduced significantly compared to the surrounding material [34]. In the simulated flow front patterns in Fig. 13, the probability for formation of a dry spot at a specific location can be assumed to increase with increasing time for the flow front to reach this location, implying that it is highest in zones indicated in red and lowest in zones indicated in blue. For the examples shown in Fig. 13, the probability to be affected by dry spot formation is significantly higher for case “unlikely” at $\sigma_\alpha = 2.5°$ than for case “on target” at $\sigma_\alpha = 2.5°$. However, this refers only to meso-/macro-scale dry spots, not to micro-scale voids which are caused by differences in flow velocity between inter-yarn gaps and yarns and capillary pressure as discussed, e.g. by Lee et al. [35]. These effects cannot be assessed here since the meso-scale fabric structure was homogenised for flow modelling.

5 Conclusion

The local fibre arrangement in a bi-directional fabric formed to a complex shape was modelled considering combined deterministic and stochastic non-uniformity in fabric properties. The stochastic arrangement of filaments within yarns, described based on experimental data, was taken into account in numerical approximation of axial and transverse yarn permeabilities. The stochastic arrangement of yarns in a fabric, which determines the

dimensions of inter-yarn gap spaces locally, was modelled as in-plane yarn waviness and related to experimentally observed fibre angle distributions. In addition, the deterministic process of fabric drape was considered here, which reduces randomness in the yarn arrangement locally through reduction of yarn mobility and yarn straightening. This is related to localised reduction of inter-yarn gap spaces during shear. To mimic the uncertainty in placing a dry reinforcement in a tool as start for the following deterministic forming process, drape simulation was randomised in terms of start point and yarn start orientations, which determine yarn paths and local fabric shear angles.

From yarn permeabilities and simulated local yarn spacing distributions, local fibre volume fractions and fabric permeabilities were approximated. Particular attention was paid to the realistic description of equivalent permeabilities of gaps between yarns with elliptical cross-section, which were expressed as a function of geometrical yarn parameters.

For demonstration of the proposed approach for generation of permeability fields, resin injection into a deformed fabric was simulated for three different drape scenarios with different probabilities and three different degrees of fabric randomness. The results indicate that variability in fabric properties and the forming process affects flow front shapes and times for complete impregnation of the reinforcement. It can be concluded that random effects need to be considered in simulations, e.g. using a Monte-Carlo approach, to allow prediction of the most probable scenarios and the range of possible outcomes.

Future work will aim at validating predicted resin flow scenarios experimentally, and the effect of non-uniform permeability fields on defect formation will be studied in detail.

Acknowledgement
This work was funded by the Engineering and Physical Sciences Research Council (grant number: EP/IO33513/1), through the EPSRC Centre for Innovative Manufacturing in Composites.

References

1. Behre B. Mechanical Properties of Textile Fabrics. Part I: Shearing. *Text Res J* 1961; 31(2): 87-93.
2. Skelton J. Fundamentals of Fabric Shear. *Text Res J* 1976; 46(1): 862-869.
3. Van der Weeën, F. Algorithms for Draping Fabrics on Doubly-Curved Surfaces. *Int J Numer Meth Eng* 1991; 31(7): 1415-1426.
4. Hammami A, Trochu F, Gauvin R, Wirth S. Directional permeability measurement of deformed reinforcement. *J Reinf Plast Comp* 1996; 15(6): 552-562.
5. Smith P, Rudd CD, Long AC. The effect of shear deformation on the processing and mechanical properties of aligned reinforcements. *Compos Sci Technol* 1997; 57(3): 327-344.
6. Lai CL, Young WB. Model resin permeation of fibre reinforcements after shear deformation. *Polym Composite* 1997; 18(5): 642-648.
7. Bickerton S, Simacek P, Guglielmi SE, Advani SG. Investigation of draping and its effect on the mold filling process during manufacturing of a compound curved composite part. *Compos Part A-Appl S* 1997; 28(9-10): 801-816.
8. Lundström TS, Frishfelds V, Jakovics A. A Statistical Approach to Permeability of Clustered Fibre Reinforcements. *J Compos Mater* 2004; 38(13): 1137-1149.
9. Endruweit A, Ermanni P. The In-Plane Permeability of Sheared Textiles. Experimental Observations and a Predictive Conversion Model. *Compos Part A-Appl S* 2004; 35(4): 439-451.
10. Hoes K, Dinescu D, Sol H, Parnas RS, Lomov S. Study of nesting induced scatter of permeability values in layered reinforcement fabrics. *Compos Part A-Appl S* 2004; 35(12): 1407-1418.
11. Endruweit A, Long AC. Influence of stochastic variations in the fibre spacing on the permeability of bi-directional textile fabrics. *Compos Part A-Appl S* 2006; 37(5): 679–694.
12. Endruweit A, McGregor P, Long AC, Johnson MS. Influence of the fabric architecture on the variations in experimentally determined in-plane permeability values. *Compos Sci Technol* 2006; 66(11-12): 1778-1792.
13. Skordos AA, Sutcliffe MPF. Stochastic simulation of woven composites forming. *Compos Sci Technol* 2008; 68(1): 283–296.
14. Abdiwi F, Harrison P, Koyama I, Yu WR, Long AC, Correia N, Guo Z. Characterising and Modelling Variability of Tow Orientation in Engineering Fabrics and Textile Composites. *Compos Sci Technol* 2012; 72(9): 1034–1041.
15. Long AC, Souter BJ, Robitaille F, Rudd CD. Effects of fibre architecture on reinforcement fabric deformation. *Plast Rubber Compos* 2002; 31(2): 87-97.
16. Elkington M, Bloom D, Ward C, Chatzimichali AP, Potter KD. Understanding the Lamination Process. In: 19th International Conference on Composite Materials. Montreal; 2013.
17. Ghanem R, Dham S. Stochastic finite element analysis for multiphase flow in heterogeneous porous media. *Transport Porous Med* 1998; 32(3): 239–262.
18. Yushanov SP, Bogdanovich AE. Fiber Waviness in Textile Composites and Its Stochastic Modeling. *Mech Compos Mater* 2000; 36(4): 297-318.
19. Weisstein EW. Inverse Erf. *MathWorld* – A Wolfram Web Resource. <http://mathworld.wolfram.com/InverseErf.html>. 1999 – 2013 Wolfram Research, Inc. (viewed 06.11.2013).
20. Olave M, Vanaerschot A, Lomov SV, Vandepitte D. Internal geometry variability of two woven composites and related variability of the stiffness. *Polym Composite* 2012; 33(8): 1335–1350.
21. Nordlund M, Lundström TS. Numerical Study of the Local Permeability of Noncrimp Fabrics. *J Compos Mater* 2005; 39(10); 929-947.
22. Endruweit A, Gommer F, Long AC. Stochastic analysis of fibre volume fraction and permeability in fibre bundles with random filament arrangement. *Compos Part A-Appl S* 2013; 49: 109–118.
23. Walther J, Simacek P, Advani SG. The effect of fabric and fiber tow shear on dual scale flow and fiber bundle saturation during liquid molding of textile composites. *Int J Mater Form* 2012; 5(1): 83-97.
24. Gebart BR. Permeability of Unidirectional Reinforcements for RTM. *J Compos Mater* 1992; 26(8): 1100-1133.
25. Weisstein EW. Ellipse. *MathWorld* - A Wolfram Web Resource. <http://mathworld.wolfram.com/Ellipse.html>. 1999-2013 Wolfram Research, Inc. (viewed 04.09.2013).
26. Mortensen NA, Okkels F, Bruus H. Reexamination of Hagen-Poiseuille flow: Shape dependence of the hydraulic resistance in microchannels. *Phys Rev E* 71 2005; 057301.
27. White FM, Fluid Mechanics, 3rd ed., New York, NY: McGraw Hill, 1994.
28. Gommer F, Endruweit A, Long AC. Non-uniformity of the filament distribution in fibre bundles and its effect on defect formation in liquid composite moulding. In: 18th International Conference on Composite Materials. Jeju Island; 2011.
29. Potluri P, Sagar TV. Compaction modelling of textile preforms for composite structures, *Compos Struct* 2008; 86(1-3): 177-185.

30. Shojaei A. A numerical study of filling process through multilayer preforms in resin injection/compression molding. *Compos Sci Technol* 2006; 66(11-12): 1546–1557.
31. Endruweit A, Ermanni P. Orientation of the permeability principal axes in bi-directional textile fabrics. *J Reinf Plast Comp* 2004; 23(10): 1063-1073.
32. Rietman B, Haanappel SP, ten Thije RHW, Akkerman R. Forming simulation sensitivity study of the double-dome benchmark geometry. *Key Eng Mat* 2012; 504-506: 301-306.
33. Trochu F, Gauvin R, Gao DM. Numerical analysis of the Resin Transfer Molding process by the finite element method. *Adv Polym Tech* 1993; 12(4): 329-342.
34. Liu B, Bickerton S, Advani SG. Modelling and simulation of resin transfer moulding (RTM) – gate control, venting and dry spot prediction. *Compos Part A-Appl S* 1996; 27(2): 135–141.
35. Lee DH, Lee WI, Kang MK. Analysis and minimization of void formation during resin transfer molding process. *Compos Sci Technol* 2006; 66(16): 3281-3289.

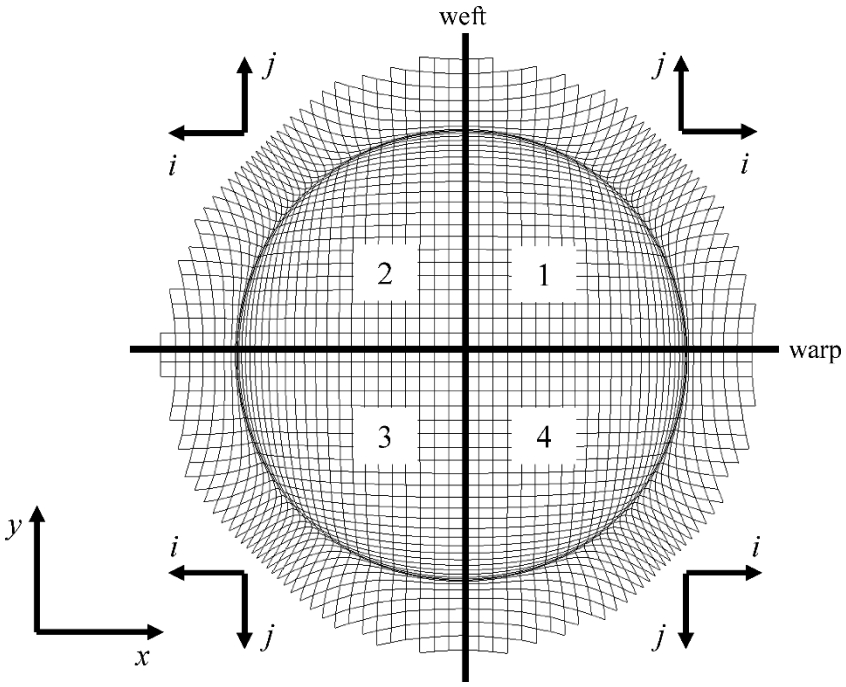

Fig. 1. Definition of quadrants relative to seed yarn paths for the example of fabric drape over a hemisphere.

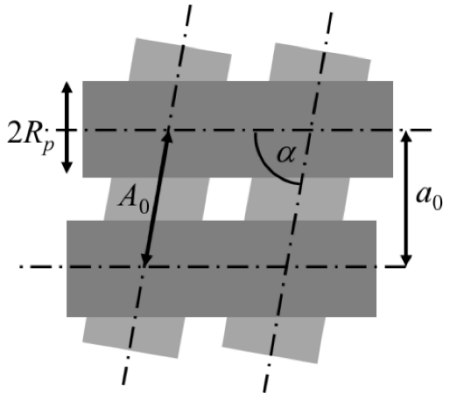

Fig. 2. Illustration of relation between yarn spacing in unsheared fabric, A_0, yarn spacing in sheared fabric, a_0, and fibre angle, α; R_p is in-plane dimension of yarns.

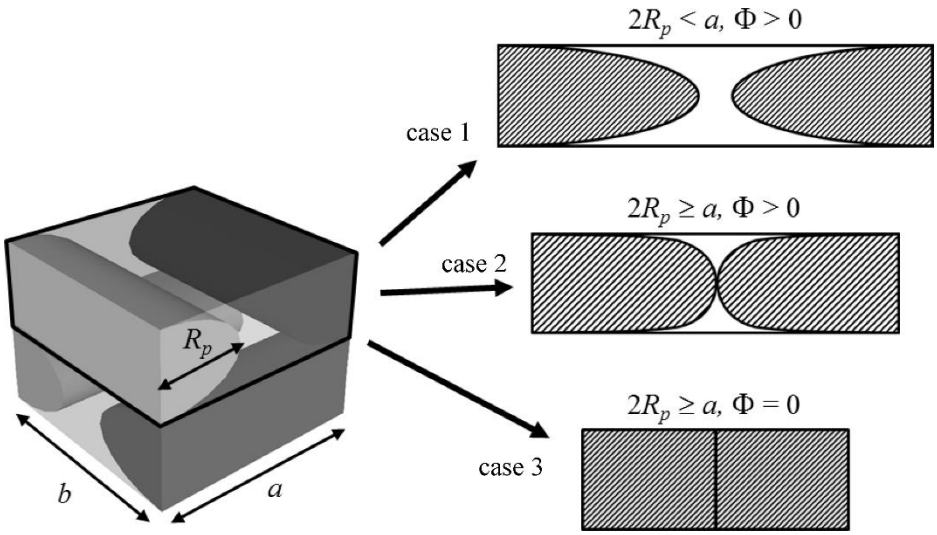

Fig. 3. Left: local approximation of fabric geometry; right: three alternative cases for approximated cross-sections of yarns and inter-yarn gaps in layer with yarn spacing, a, and original yarn halfwidth, R_p, in the undeformed fabric.

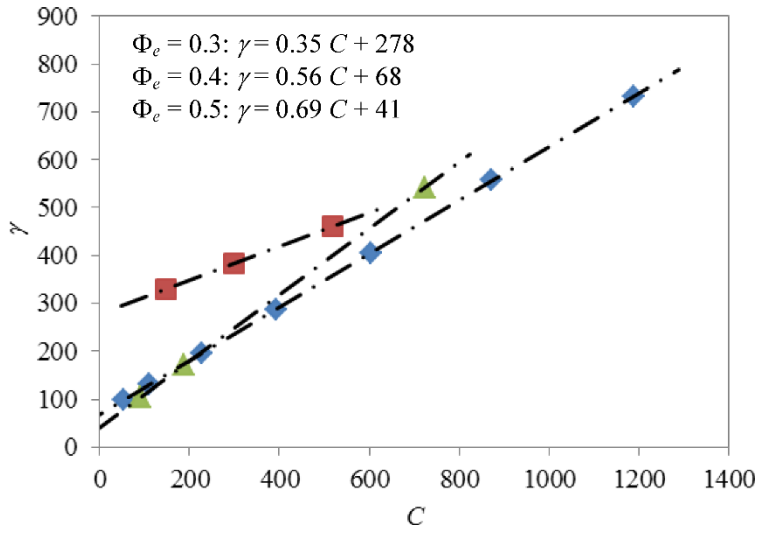

Fig. 4. Geometrical correction factor, γ, as a function of the duct compactness, C, for different percentages Φ_e; square symbols: $\Phi_e = 0.30$; diamond symbols: $\Phi_e = 0.40$; triangular symbols: $\Phi_e = 0.50$.

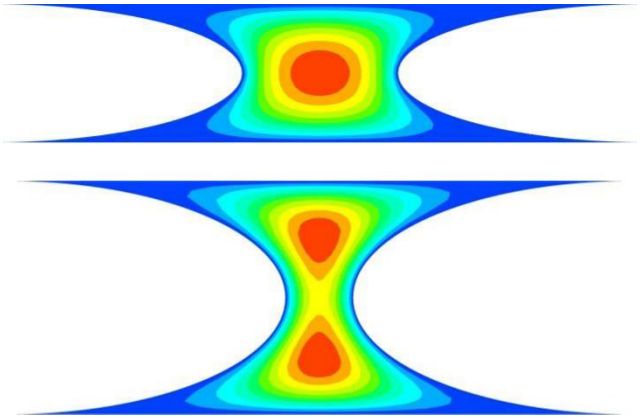

Fig. 5. Results of CFD simulations: Contours indicating qualitatively different axial flow velocity distributions in inter-yarn gaps (elliptical yarns) for different values of Φ_e; top: $\Phi_e = 0.40$; bottom: $\Phi_e = 0.30$.

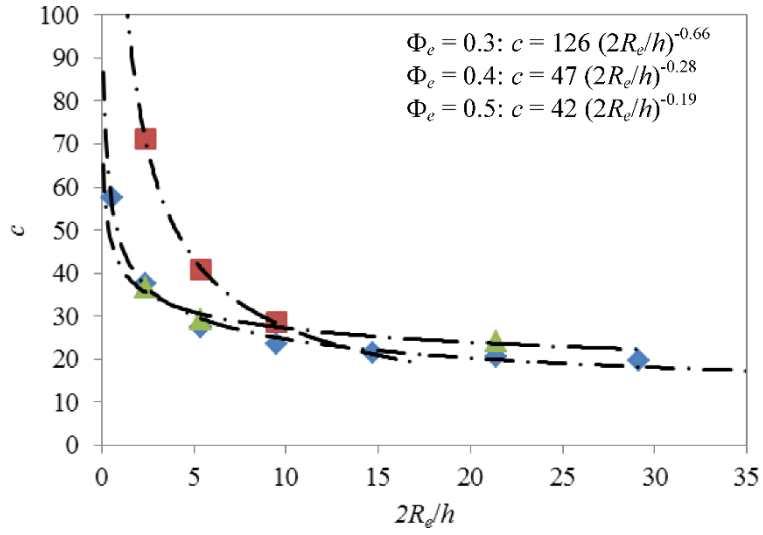

Fig. 6. Friction factor, c, as a function of aspect ratio, $2R_e/h$, of the elliptical yarns for different percentages Φ_e; square symbols: $\Phi_e = 0.30$; diamond symbols: $\Phi_e = 0.40$; triangular symbols: $\Phi_e = 0.50$.

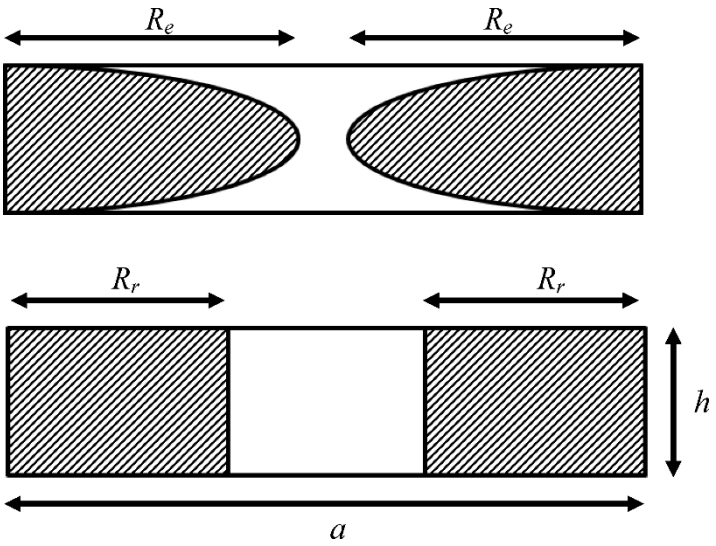

Fig. 7. Repetitive cross-sectional unit of each layer of yarns in a simplified bi-directional fabric; top: approximately elliptical geometry of yarns (shaded) and inter-yarn gap (white); bottom: abstracted rectangular geometry for permeability estimation.

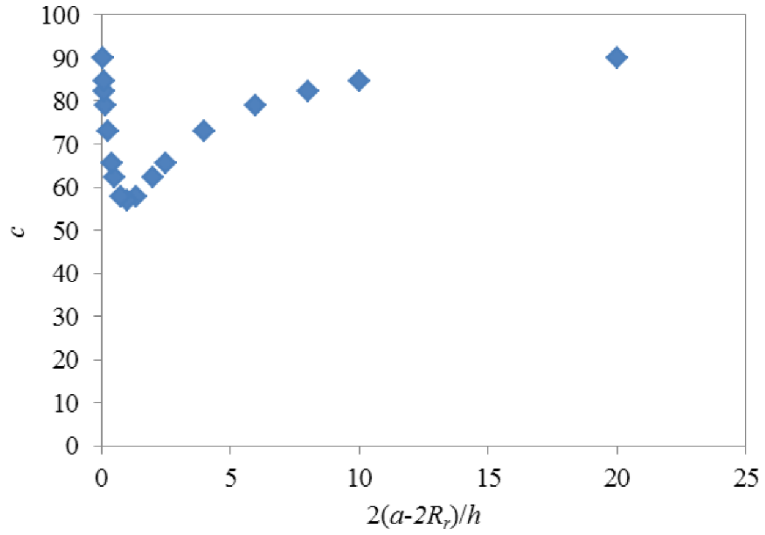

Fig. 8. Values for friction factor, c, according to White [27] as a function of aspect ratio, $2(a\text{-}2R_r)/h$, of the rectangular gaps.

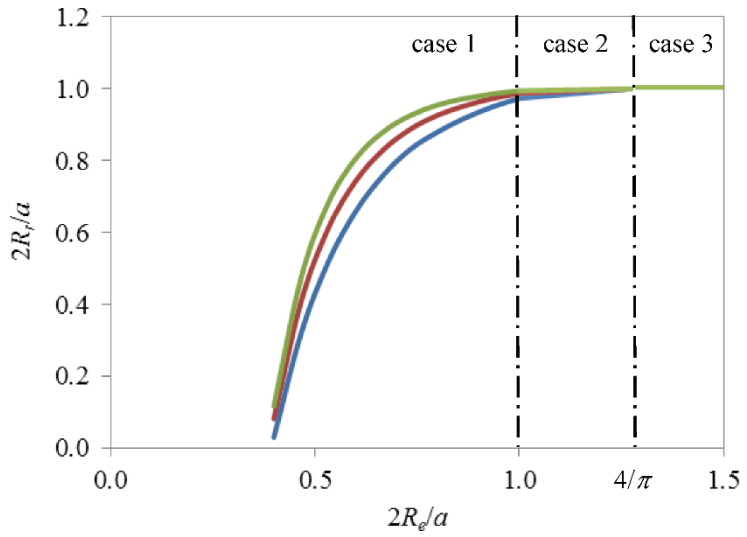

Fig. 9. Dependence of R_r on R_e for different ratios a/h; top curve: a/h = 12; middle curve: a/h = 6; bottom curve: a/h = 3.

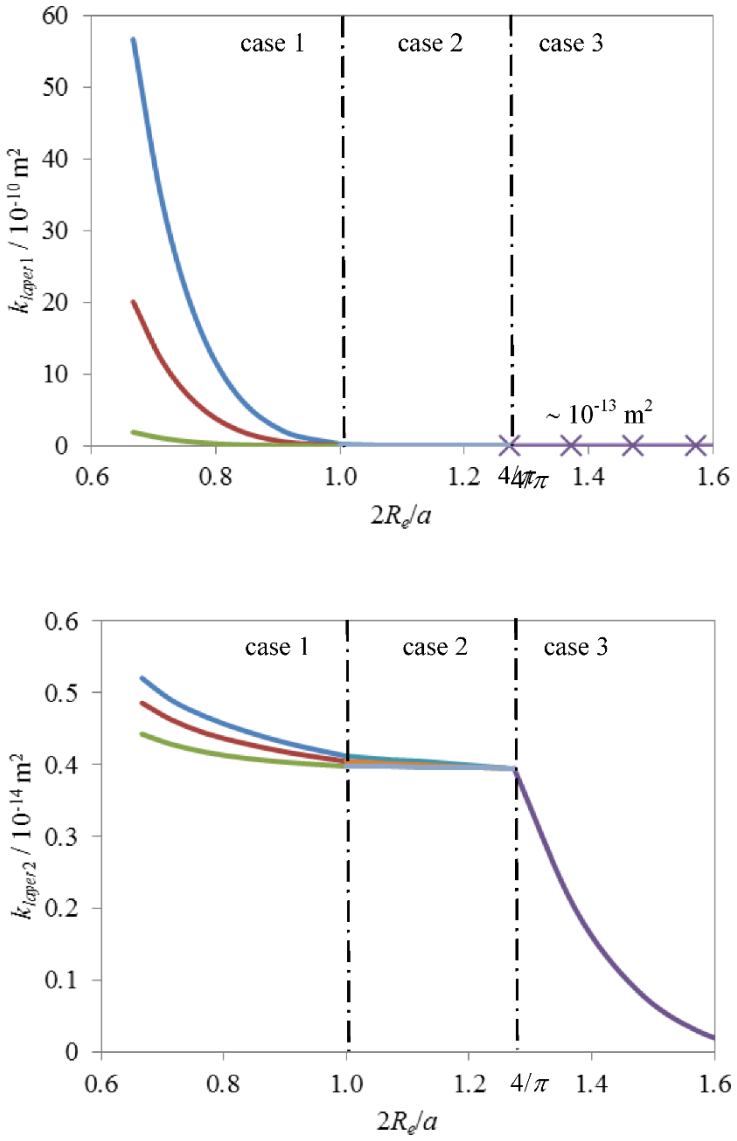

Fig. 10. Calculated layer permeabilites, k_{layer1} and k_{layer2} for different ratios h/R_e; top curve: h/R_e = 1.0; middle curve: h/R_e = 0.6; bottom curve: h/R_e = 0.2.

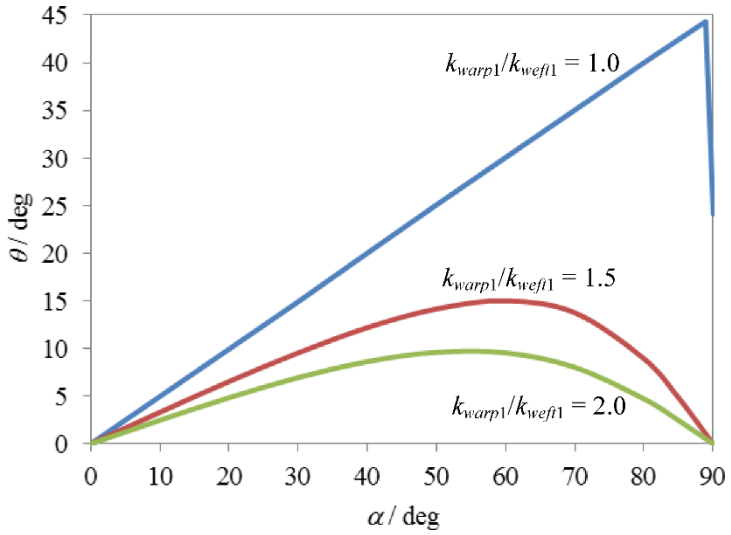

Fig. 11. Angle θ, characterising the orientation of the principal flow direction relative to the warp direction in the fabric as a function of the inter-yarn angle, α; for all curves: $k_{warp2} = k_{weft2}$ and $k_{weft1} = 2 \times k_{weft2}$; parameter k_{warp1}/k_{weft1}.

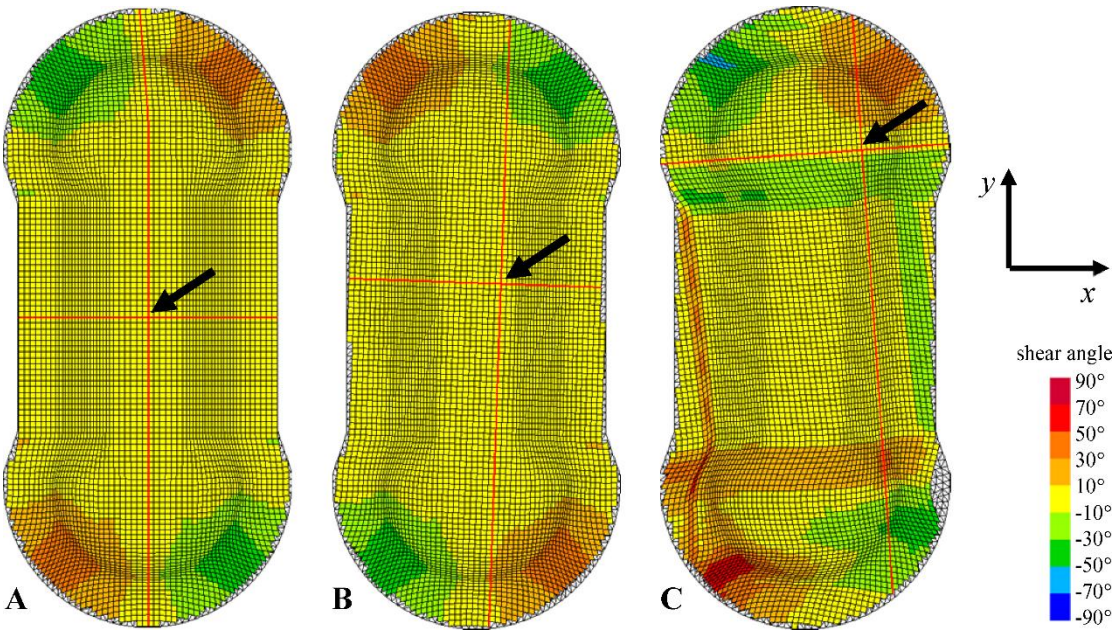

Fig. 12. Shear angle distributions for double-dome (forming benchmark) geometry at different scenarios; A: on target; B: likely; C: unlikely; arrows indicate start point for drape simulation; length of geometry along *y*-direction is 360 mm.

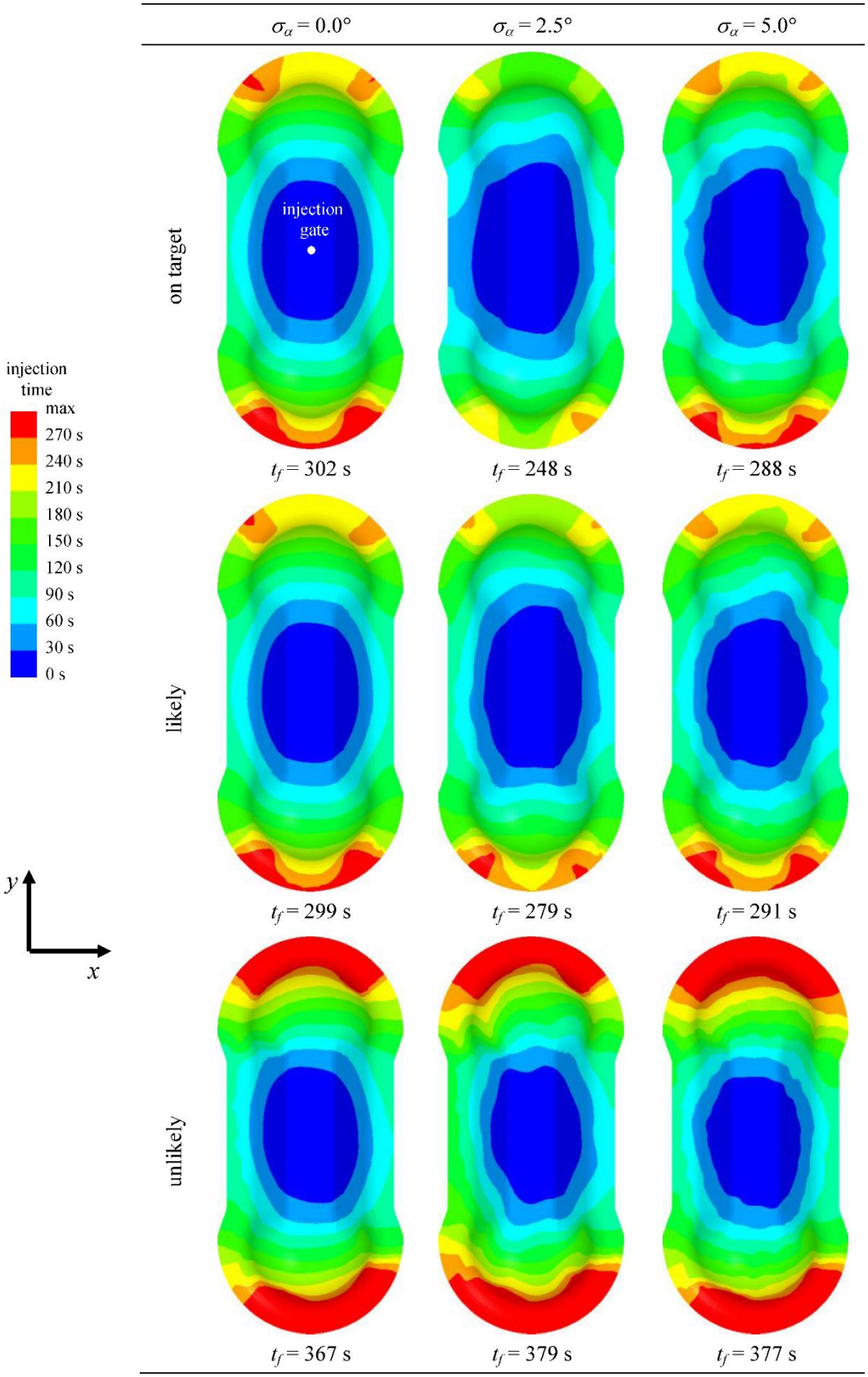

Fig. 13. Typical examples for flow front positions at different injection times; total fill times, t_f, are also given.

Table 1. Conversion of positive integers, i and j, indexing yarn cross-over points in each quadrant to unique signed integers, n_{warp} and n_{weft}.

quadrant	n_{warp}	n_{weft}
1	i	j
2	$-i$	j
3	$-i$	$-j$
4	i	$-j$

Table 2. Geometrical yarn parameters in Eqs. (32) and (33); V_{fmax} determined from theoretical considerations, $R_f^2/4c_1$ and $c_2R_f^2$ determined from comparison with numerically generated yarn permeability data [22].

V_{fmax}	$R_f^2/4c_1$	$c_2R_f^2$
0.91	5.69×10^{-12} m^2	27.49×10^{-14} m^2

Table 3. Parameters characterising architecture of undeformed uniform fabric: yarn spacing, A_0, yarn halfwidth, R_e, ratio A_0/R_e, yarn thickness, h, fibre volume fraction, V_f, isotropic permeability, K.

A_0 / mm	R_e / mm	A_0 / R_e	h / mm	V_f	K / 10^{-10} m^2
3.36	1.40	2.4	0.50	0.54	8.15

Table 4. Characterisation of start configuration for drape simulation: co-ordinates of start point, x and y, angle describing surface normal, β, and probability relative to probability to start on target, dP_{xy}/dP_{xy0}; deviation of yarn orientations from target start orientation is also given.

	x / mm	y / mm	β	dP_{xy}/dP_{xy0}	deviation from target orientation
on target	0.0	0.0	0°	1.00	0°
likely	15.5	20.5	0°	0.88	-2°
unlikely	33.4	97.3	35°	0.10	4°

Table 5. Total fill times for different combinations of drape scenario and standard deviation of fibre angles, σ_α; average values, standard deviations and coefficients of variation (standard deviation / average value) are given where appropriate.

	total fill times / s		
	$\sigma_\alpha = 0.0°$	$\sigma_\alpha = 2.5°$	$\sigma_\alpha = 5.0°$
on target	302	244 ± 30 (± 12 %)	292 ± 13 (± 4 %)
likely	299	284 ± 15 (± 5 %)	303 ± 28 (± 9 %)
unlikely	367	377 ± 44 (± 11 %)	377 ± 28 (± 7 %)